

© 2019 The Authors Published by the European Association of Geochemistry

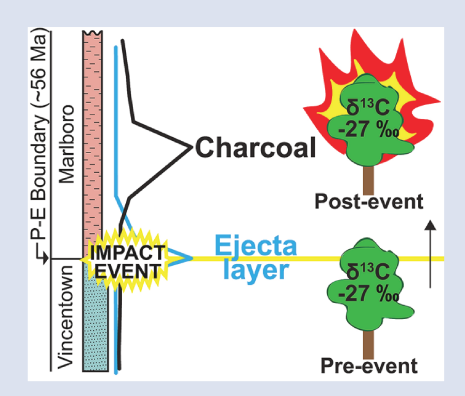
Widespread and intense wildfires at the Paleocene-Eocene boundary

M.K. Fung^{1*}, M.F. Schaller¹, C.M. Hoff¹, M.E. Katz¹, J.D. Wright²



Abstract

doi: 10.7185/geochemlet.1906



Discovery of impact spherules associated with the onset of the Carbon Isotope Excursion (CIE) that marks the Paleocene-Eocene (P-E) boundary (~56 Ma) indicates that the P-E transition was coincident with an extraterrestrial impact. Charcoal abundances increase >20 times background immediately above the P-E spherule layer at two Atlantic Coastal Plain palaeo-continental shelf localities located >200 km apart. Individual charcoal shards (~100 μm long; 58-83 wt. % carbon) show charred plant features. The carbon isotope ratio of charcoal $(\delta^{13}C_{charcoal})$ through the peak shows that it originated from pre-impact vegetation that burned. We consider two scenarios to explain this widespread, synchronous increase in charcoal at the P-E boundary: 1) warming-induced, continental-scale drying; and 2) impact-induced wildfires. Differentiating between these two hypotheses depends critically on the observed sequence of events, which on the western North Atlantic margin is: the impact spherule horizon, followed by the peak in charcoal (derived from vegetation that grew before the CIE and impact),

and finally the nadir of the CIE. Importantly, the pre-excursion δ^{13} C _{charcoal} remains constant through the CIE onset, requiring a dramatic increase in sedimentation. This work clarifies our understanding of the timing and sequence of events following an extraterrestrial impact at the P-E boundary.

Received 13 November 2018 | Accepted 28 January 2019 | Published 1 March 2019

Introduction

The P-E boundary is marked by a negative CIE in marine and terrestrial records and 5-8 °C global warming (Kennett and Stott, 1991; see McInerney and Wing, 2011, for review). Although the source(s) and magnitude of low δ¹³C carbon released into the ocean-atmosphere system at the P-E boundary are debated, impact ejecta recently discovered at the CIE onset indicates that an extraterrestrial impact played a role. Glassy spherules are found in a discrete stratigraphic layer within the CIE onset on the U.S. Atlantic Margin at multiple sites spread over 1,000 km (Schaller et al., 2016). The ejecta at Wilson Lake B (WL; Schaller et al., 2016) and at Randall's Farm (RF; this study, Fig. S-1) are formed as either solidified melt-droplets or vapour condensates. On the palaeo-continental shelf, the CIE onset coincides with the base of the thick Marlboro Clay that extends from Virginia to New Jersey (Fig. 1).

In this study, we document unusually abundant microscopic (~100 µm) black charcoal shards near the base of the Marlboro Clay at WL and RF; these shards bear characteristics of well-preserved charred plant material and their distribution in the sediment column forms an abrupt peak immediately above the spherule level. SEM imaging – the most diagnostic method of studying charcoalified plant material (Scott and Collinson, 1978) – reveals three-dimensional plant features with excellent preservation, including homogeneous cell walls and honeycomb structures (Figs. 2, S-2). This paper explores two hypotheses for the origin of the charcoal following the impact ejecta within the CIE: 1) warming-induced, continental drying and ecosystem change; and 2) as a direct consequence of the impact.

Evidence for Synchronous, Widespread Intense Wildfires

Charcoal is the most diagnostic artefact of wildfires (Belcher et al., 2003). Overlying the P-E impact ejecta, we observe a 24-fold increase in charcoal pieces (>63 µm)/gram at WL, and 21-fold increase at RF, a remarkable change above a low but consistent background (Figs. 3, S-3). The material is typically brittle, black, opaque in thin section, and preserves anatomical detail. Raman spectroscopy is widely used to characterise carbonaceous materials (Ulyanova et al., 2014; Wang et al., 2014), and helps confirm the presence of charcoal (Fig. S-4). Wavelength dispersive X-ray spectroscopy (WDS) indicates that the black shards are 58-84 % carbon by weight. Charcoal

Corresponding author (e-mail: megankfung@gmail.com)



Department of Earth and Environmental Sciences, Rensselaer Polytechnic Institute, Troy, NY 12180, USA

Department of Earth and Planetary Sciences, Rutgers University, Piscataway, NJ 08854, USA

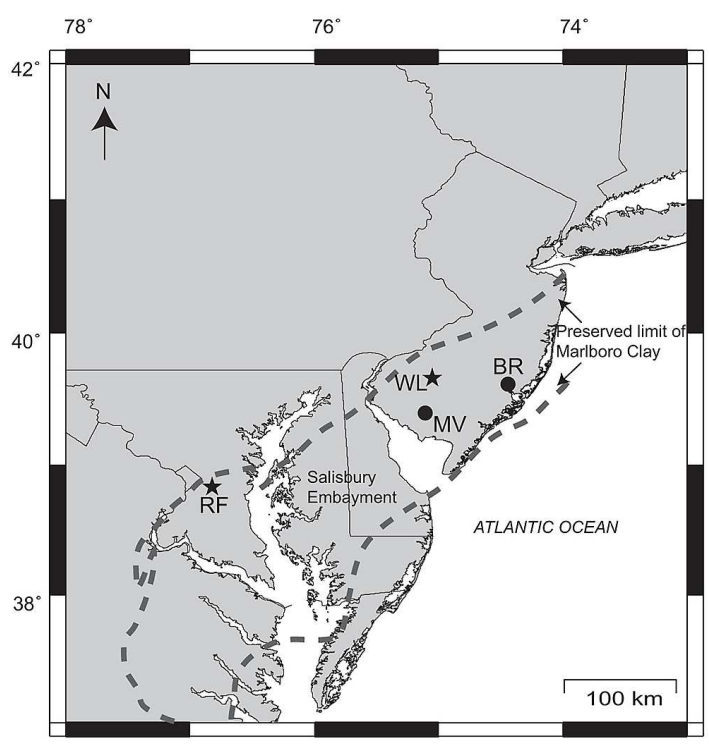


Figure 1 Location map of Wilson Lake (WL), Randall's Farm (RF) and other sites discussed in text; Millville (MV), Bass River (BR). Modified after Self-Trail (2017).

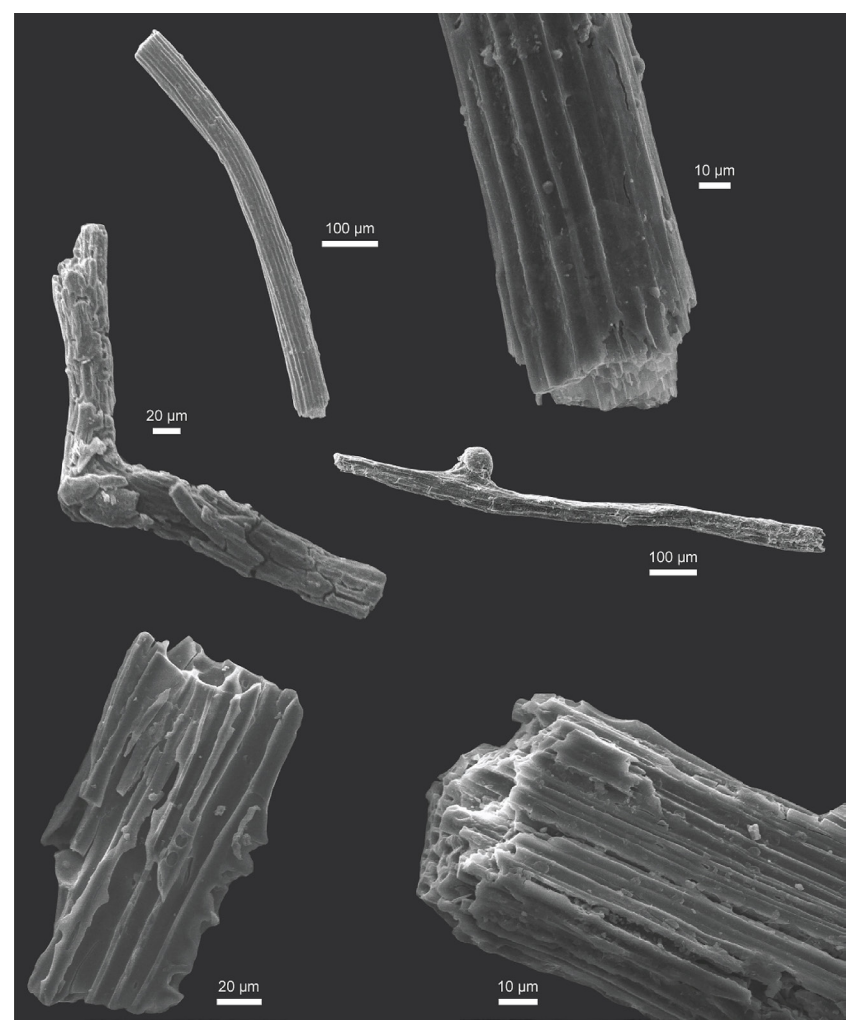


Figure 2 SEM images of charcoal fragments from WL and RF.



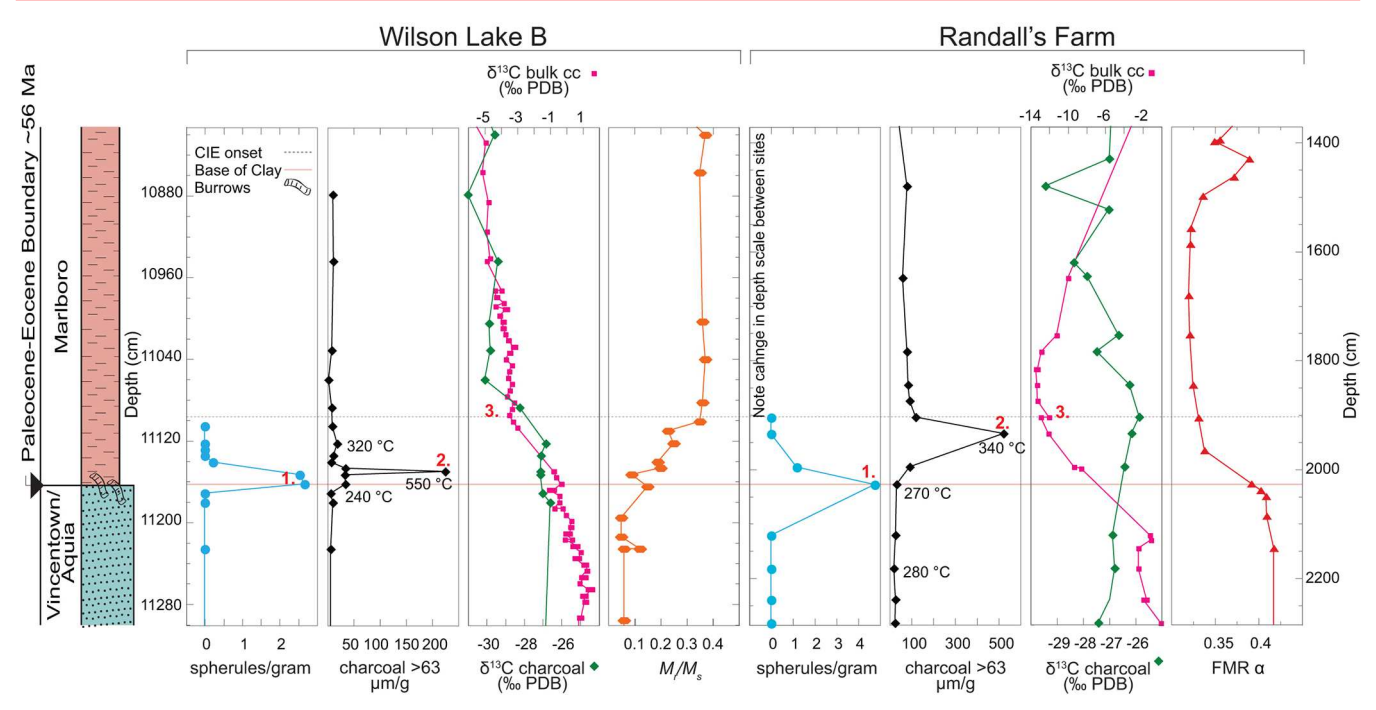
exhibits high reflectance (R_o) compared to other maceral groups as the result of heating; higher reflectance indicates higher combustion temperatures (Scott and Jones, 1991). Samples yield average R_o values between 0.38 % and 2.99 %, corresponding to temperatures between 340-550 °C (Scott and Jones, 1991) (Table S-1). Lowest R_o values indicating vitrinite (uncharred plant material) are found below the boundary; highest R_o values occur within the charcoal peak at both RF (1.24 %) and WL (2.99 %), and decrease above; this distribution of R_o values supports a widespread and intense singular wildfire event.

The ejecta found at the base of the Marlboro Clay, have all the characteristics of instantaneous air-fall deposit (Schaller *et al.*, 2016), and have been dated by K-Ar to 54.9 ± 3 Ma (Schaller and Fung, 2018). Because the depositional and cooling ages of the spherules appear to be indistinguishable, the impact ejecta may provide a time-equivalent marker and baseline for the start of the CIE across the mid-Atlantic Salisbury Embayment. The charcoal peak at both localities occurs stratigraphically above both the spherule layer and the start of the CIE; based on this sequence, we infer that: 1) the charcoal was deposited after the impact; and 2) synchronous wildfires produced the charcoal.

Several lines of evidence indicate that the charcoal-rich layers are neither artefacts of reworked older sediments nor simply due to sedimentation change. (1) The charcoal peak lies 12 and 104 cm above the ejecta layer at WL and RF, respectively, indicating that the charcoal is not older burned material reactivated by the impact event. (2) The charcoal increases substantially above the change from sands to clayey silts, and decreases to near-background levels well within the clay. (3) There is a single observed pulse of charcoal, not multiple peaks as would be expected from reworking of charcoal.

There is a stratigraphic and causal link between our charcoal observations and an unusual and widespread abundance of magnetic nanoparticles in the Marlboro Clay (Lanci et al., 2002), which resulted from soil pyrogenesis (Kent et al., 2017). The stratigraphic level of the charcoal increase at RF and WL coincides with this unique change in magnetisation (Kopp et al., 2009 and Kent et al., 2017, respectively; Fig. 3), indicating that they share a common origin and were deposited contemporaneously. The unique magnetisation is observed in ten sites spanning ~400 km in the Salisbury Embayment (Kopp et al., 2009), providing an independent line of evidence indicating that the wildfire activity was regionally extensive (See SI). Elevated fern spores and charred plant material within the CIE at the Mattawoman Creek-Billingsley Road site in the southern Salisbury Embayment (Self-Trail et al., 2017) provides further evidence that the wildfires were widespread and contemporaneous (within the level of resolution possible). The dramatic increase and dominance of fern spores in the Marlboro Clay is consistent with the opportunistic nature of ferns immediately following wildfire (Ainsworth and Kauffman, 2009).

We use the nadir of the CIE onset as a tie point to correlate the sequence of events recorded at WL and RF (Fig. 3). Remarkably, the highest charcoal abundance occurs prior to the CIE nadir, highlighting the following sequence of events: 1) impact event (deposition of spherule layer); 2) widespread wildfires (significant increase in charcoal); and 3) CIE nadir. The significant increase in charcoal invites the obvious question: what triggered the intense, widespread wildfires that produced the charcoal spike? Here, we consider two scenarios to explain the elevated charcoal abundance at the P-E boundary: 1) continental drying and subsequent wildfires; and 2) impact-induced wildfires.



Ratio of saturation remanence to saturation magnetisation (M_r/M_s) --- Ferromagnetic resonance spectroscopy (FMR α)

Base of Marlboro Clay/spherule peak and CIE nadir are used as tie points between sites

Figure 3 Charcoal abundance (# >63 µm/gram) and $\delta^{13}C_{charcoal}$ (this study) plotted with $\delta^{13}C_{bulk\ carbonate}$ and spherules/gram discovered at WL (Schaller *et al.*, 2016) and RF (this study). Total depth range at RF is ~2 times WL, allowing for direct comparison. Note difference in isotope scale between WL and RF. R_o measurements, Mr/Ms at WL (Kent *et al.*, 2017), and FMR α at RF (Kopp *et al.*, 2009) are shown.



Scenario 1: Warming-induced, continental drying and subsequent wildfires

Large scale continental drying associated with Paleocene-Eocene Thermal Maximum (PETM) warming could put vegetation at risk for wildfires. These wildfires could be triggered by lightning strikes and be regionally widespread. The first of these many fires would burn extensively, probably contemporaneously, over a wide area, be very intense, and lead to deposition of the large charcoal peak we observe in the sedimentary record. This would likely be followed by subsequent smaller wildfire events producing repeated charcoal pulses, which we do not observe.

Under this scenario, continental interiors experienced aridification. Studies from the U.S. western interior indicate rainfall decreased by ~40 % near the PETM onset, but do not conclude if this aridification was more than regional (Wing et al., 2005). Palaeosols in Wyoming also indicate decreased precipitation at the onset (Kraus and Riggins, 2007). Conversely, modelling results from northern and mid-latitudes (including Wyoming) indicate a 20-25 % increase in soil and atmospheric moisture during the PETM (Bowen et al., 2004), and Kopp et al. (2009) speculated on an "Appalachian Amazon" in Eastern North America. The latter is consistent with the apparent runoff increase responsible for the Apectodinium acme at the P-E onset in the Marlboro Clay (Sluijs et al., 2007). Hydrologic studies on the PETM thus have not provided clear evidence for a pattern of dryer or wetter conditions, but observations suggest the mid-Atlantic margin was wet.

Scenario 2: Impact-induced wildfires

The charcoal peaks at WL and RF occur stratigraphically above the ejecta layer; therefore, the wildfires could have been ignited by the P-E boundary impact. In this scenario, the massive thermal energy of an impact vapour plume and subsequent ejecta fallout (Melosh *et al.*, 1990) ignited widespread wildfires, producing abundant charcoal that was transported to the shelf *via* the next major hydrologic event, resulting in the observed depositional sequence. Wildfires following the Cretaceous-Paleogene boundary impact event (see SI for review) provide a model for the P-E boundary impact and potential ignition mechanism, though we note that the P-E boundary impact was smaller.

The $\delta^{13}C_{charcoal}$ at WL and RF provides insight into our two proposed wildfire ignition scenarios and sequence of events (Fig. 3). The $\delta^{13}C_{charcoal}$ from the charcoal peak exhibits pre-excursion values, and $\delta^{13}C_{\text{charcoal}}$ remains constant through the start of the CIE onset in bulk carbonate. Pre-excursion δ¹³C_{charcoal} values indicate that: 1) the charcoal peak resulted from biomass that grew prior to the impact event and climatic perturbation; and 2) there was no vegetation growth within the time represented by the section of steady $\delta^{13}C_{charcoal}$ values through the CIE onset and charcoal peak. If the vegetation had grown during the CIE onset, as expected during a millennial-scale event, the $\delta^{13}C_{charcoal}$ would display excursion values because new plant growth would record the changing atmospheric δ^{13} C. In contrast, our δ^{13} C_{charcoal} decreases above peak charcoal abundance and above the start of the CIE onset in bulk carbonate. At WL, two low charcoal abundance samples above the peak exhibit pre-excursion $\delta^{13}C_{charcoal}$ values, hence the pre-excursion $\delta^{13}C_{charcoal}$ values in the charcoal peak do not represent a mixture of pre-excursion and excursion carbon, diluted by an over-abundance of pre-excursion vegetation that burned along with it. Because there was apparently no time for new plant growth, we conclude that sediment deposition between the impact ejecta and the $\delta^{13}C_{charcoal}$ excursion was relatively fast (no more than centennial scale).

Climate Change or Impact Event?

Under the drying scenario, the climate must have become hotter and drier as a result of the carbon cycle event. The environmental perturbation and warm temperatures associated with the PETM created conditions favourable for wildfires, yet peak charcoal occurs within the start of the onset and before the nadir of the excursion, which coincides with most observations of environmental perturbation. This suggests that the PETM climate perturbation did not cause the widespread wildfires and charcoal deposition; rather, wildfires were the consequence of an earlier event. The drying scenario is also inconsistent with the apparent massive increase in sedimentation rate at Salisbury Embayment shelf sections, which would have required an accelerated hydrologic cycle and increased precipitation and runoff, although we note that wildfires would result in significant soil loss. Interestingly, fern spikes of up to 90 % within the Marlboro Clay in the southern Salisbury Embayment suggest warm, wet environments (Self-Trail et al., 2017) because ferns need moist environments to complete their lifecycle (Mehltreter et al., 2010), making them particularly rare in arid climates (Aldasoro et al., 2004). If drying were the source of the P-E boundary wildfires, then there should be evidence of fires during subsequent Early Eocene Hyperthermal events, yet charcoal studies through the Early Eocene Climatic Optimum in Germany do not indicate any increase in fire activity (Robson et al., 2014).

Although our findings are most consistent with impact-induced wildfires at the P-E boundary, either ignition scenario is feasible. Importantly, both continental drying and impact-induced wildfires are in agreement with a fast scenario (Wright and Schaller, 2013), supported by δ¹³C_{charcoal} analyses. In contrast, a 4 kyr onset (Zeebe et al., 2016) requires the absence of plant growth or wildfires in the hinterlands for thousands of years; this is unlikely because fire has a revitalising effect on ecosystems and vegetation growth is quickly renewed following wildfires (Ahlegren, 1974). A sustained period without vegetative growth or wildfires for millennia is highly improbable (Bond and Wilgen, 1996) when the lifetime of a typical large woody plant is less than a few centuries; therefore, we would expect resumption of at least background charcoal flux with post-CIE δ¹³C values during those millennia, which is not observed (Fig. 3). The charcoal record could consist of a mixture of charcoal that burned over a number of years; decades seem feasible, yet thousands of years is extremely unlikely, because we would expect to see multiple pulses of charcoal in the record (especially in proximal site RF), which we do not. The charcoal is so well preserved and displays such delicate features that we find it unlikely the material remained exposed on the landscape for thousands of years before being aggregated by floods.

A more realistic explanation of the charcoal record is that the P-E boundary sediments were deposited relatively rapidly during the start of the CIE onset. This explanation is consistent with mechanics of charcoal production and transport (see SI). Extremely high sedimentation rates are common in response to widespread landscape clearance by forest fires, resulting in massive post-wildfire debris flows and deposition of large volumes of sediment (Wells, 1987). Modern fires increase soil erosion rates by ~30-fold compared to pre-fire levels (Swanson, 1981). In addition, rapid mud accumulation rates are observed in the modern Amazon shelf (Kuehl et al., 1986), demonstrating that high sedimentation rates during the CIE onset are plausible, especially during an enhanced hydrologic cycle (Kopp et al., 2009) with ample sediment supply. Effects of wildfires in coastal California show a significant increase in sediment yield, and up to ~35 times greater than average during the subsequent wetter year (Warrick et al., 2012). These studies



highlight how an increase in sedimentation and erosion rates occurs during the next major hydrologic event and is therefore an immediate (decadal scale) consequence of wildfires; this provides a framework for our fast sedimentation model. Regardless of the trigger mechanism, burnt terrestrial plant matter and eroded forest soils were transported to continental shelves in a sediment deluge during the next storm event, producing the base of the Marlboro Clay (see SI).

To summarise, a synchronous, more than twenty-fold increase in charcoal abundance is identified at the P-E boundary in two locations, indicating that intense widespread wildfires occurred during a climatic warming event. We consider two hypotheses to explain the source of the wildfires: 1) warming-induced, continental drying during the PETM; and 2) thermal radiation and/or ejecta fallout from the P-E boundary impact event. Although we cannot definitively rule out either scenario, our data strongly support the impact-induced wildfire hypothesis. Regardless of the trigger mechanism, a critical finding of this study is that the carbon isotope composition of individual charcoal grains exhibit pre-excursion values and remain constant through the onset of the carbon isotope excursion, indicating a rapid onset of the CIE that challenges the rate paradigm for the very early stages of the event by thousands of years.

Acknowledgements

We thank D. Kent, K. Miller, and W. Broecker for helpful discussions, and two anonymous reviewers for their thoughtful suggestions. We express our gratitude to M. Mastalerz from Indiana University for reflectance measurements. Funding was provided by the Comer Family Foundation, and NSF award #1737100.

Editor: Sophie Opfergelt

Additional Information

Supplementary Information accompanies this letter at http://www.geochemicalperspectivesletters.org/article1906.



This work is distributed under the Creative Commons Attribution Non-Commercial No-Derivatives 4.0 License, which permits unre-

stricted distribution provided the original author and source are credited. The material may not be adapted (remixed, transformed or built upon) or used for commercial purposes without written permission from the author. Additional information is available at http://www.geochemicalperspectivesletters.org/copyright-and-permissions.

Cite this letter as: Fung, M.K., Schaller, M.F., Hoff, C.M., Katz, M.E., Wright, J.D. (2019) Widespread and intense wild-fires at the Paleocene-Eocene boundary. *Geochem. Persp. Let.* 10, 1–6.

References

- AHLEGREN, C.E. (1974) Introduction. In: Kozlowski, T.T., Ahlgren, C.E. (Eds) *Fire and Ecosystems*. Academic Press, New York, 1-5.
- AINSWORTH, A., KAUFFMAN, J.B. (2009) Response of native Hawaiian woody species to wildfires in tropical forests and scrublands. *Plant Ecology* 201, 197-209.
- ALDASORO, J.J., CABEZAS, F., AEDO, C. (2004) Diversity and distribution of ferns in sub-Saharan Africa, Madagascar and some islands of the South Atlantic. *Journal of Biogeography* 31, 1579-1604.

- Belcher, C.M., Collinson, M.E., Sweet, A.R., Hildebrand, A.R., Scott, A.C. (2003) Fireball passes and nothing burns The role of thermal radiation in the Cretaceous-Tertiary event: Evidence from the charcoal record of North America. *Geology* 31, 1061-1064.
- BOND, W.J., VAN WILGEN, B. (1996) Fire and plants. Chapman and Hall, London.
- BOWEN, G.J., BEERLING, D.J., KOCH, P.L., ZACHOS, J.C., QUATTLEBAUM, T. (2004) A humid climate state during the Palaeocene/Eocene thermal maximum. *Nature* 432, 495-499.
- KENNETT, J.P., STOTT, L.D. (1991) Abrupt deep-sea warming, palaeoceanographic changes and benthic extinctions at the end of the Palaeocene. *Nature* 353, 225-229.
- KENT, D.V., LANCI, L., WANG, H., WRIGHT, J.D. (2017) Enhanced magnetization of the Marlboro Clay as a product of soil pyrogenesis at the Paleocene-Eocene Boundary? Earth and Planetary Science Letters 473, 303-312.
- KOPP, R.E., SCHUMANN, D., RAUB, T.D., POWARS, D.S., GODFREY, L.V., SWANSON-HYSELL, N.L., MALOOF, A.C., VALI, H. (2009) An Appalachian Amazon? Magnetofossil evidence for the development of a tropical river-like system in the mid-Atlantic United States during the Paleocene-Eocene thermal maximum. *Paleoceanography* 24, PA4211.
- KRAUS, M., RIGGINS, S. (2007) Transient drying during the Paleocene–Eocene Thermal Maximum (PETM): analysis of paleosols in the bighorn basin, Wyoming. Palaeogeography Palaeoclimatology Palaeoecology 245, 444-461.
- Kuehl, S.A., Demaster, D.J., Nittrouer, C.A. (1986) Nature of sediment accumulation on the Amazon continental shelf. *Continental Shelf Research* 6, 209-225.
- LANCI, L., KENT, D.V., MILLER, K.G. (2002) Detection of Late Cretaceous and Cenozoic sequence boundaries on the Atlantic coastal plain using core log integration of magnetic susceptibility and natural gamma ray measurements at Ancora, New Jersey. *Journal of Geophysical Research* 107, 2216.
- MCINERNEY, F.A., WING S.L. (2011) Thermal Maximum: A Perturbation of Carbon Cycle, Climate, and Biosphere with Implications for the Future. Annual Review of Earth and Planetary Sciences 39, 489-516.
- MEHLTRETER, K., WALKER, L., SHARPE, J. (2010) Fern ecology. Cambridge University Press, Cambridge.
- MELOSH, H.S., SCHNEIDER, N.M., ZAHNLEK, J., LATHAM, D. (1990) Ignition of global wildfires at the Cretaceous/Tertiary boundary. *Nature* 343, 251-254.
- ROBSON, B.E., COLLINSON, M.E., RIEGEL, W., WILDE, V., SCOTT, A.C., PANCOST, R.D. (2014) A record of fire through the Early Eocene. Rendiconti Online Societa Geologica Italiana 31, 187-188.
- SCHALLER, M.F., FUNG, M.K., WRIGHT, J.D., KATZ, M.E., KENT, D.V. (2016) Evidence of an Extraterrestrial Impact at the Paleocene-Eocene boundary. Science 354, 225-229.
- SCHALLER, M.F., FUNG, M.K. (2018) The extraterrestrial impact evidence at the Paleocene-Eocene boundary and sequence of environmental change on the continental shelf. *Philosophical Transactions of the Royal* Society A 376, doi: 10.1098/rsta.2017.0081.
- SCOTT, A.C., COLLINSON, M.E. (1978) Organic sedimentary particles: results from SEM studies of fragmentary plant material. In: Whalley, W.B. (Eds) SEM in the Study of Sediments. Geoabstacts, Norwich, 137–167.
- Scott, A.C., Jones, T.P. (1991) Microscopic observations of Recent and fossil charcoal. *Microscopy and Analysis* 25, 13-15.
- Self-Trail, J.M., Robinson, M.M., Bralower, T.J., Sessa, J.A., Hajek, E.A., Kump, L.R., Trampush, S.M., Willard, D.A., Edwards, L.E., Powars, D.S., Wandless, G.A. (2017) Shallow marine response to global climate change during the Paleocene-Eocene Thermal Maximum, Salisbury Embayment, USA. *Paleoceanography and Paleoclimatology* 32, 710-728.
- SLUIJS A., BRINKHUIS, H., SCHOUTEN, S., BOHATY, S.M., JOHN, C.M., ZACHOS, J.C., REICHART, G.-J., SINNINGHE DAMSTÉ, J.S., CROUCH, E.M., DICKENS, G.R. (2007) Environmental precursors to rapid light carbon injection at the Paleocene/Eocene boundary. *Nature* 450, 1218-1221.
- SWANSON, F.J. (1981) Fire and geomorphic processes. In: Mooney, H.A., Bonniksen, T.H., Christensen, N.L., Lotan, J.E., Reiners, W.A. (Eds) Fire Regimes and Ecosystem Properties. USDA Forest Service General Technical Report WO-26.
- ULYANOVA, E.V., MOLCHANOV, A.N., PROKHOROV, I.Y., GRINYOV, V.G. (2014) Fine structure of Raman spectra in coals of different rank. *International Journal of Coal Geology* 121, 37-43.
- WANG, S., CHENG, H., JIANG, D., HUANG, F., SU, S., BAI, H. (2014) Raman spectroscopy of coal component of Late Permian coals from Southern China. Spectroscopy 132, 767-770.



- WARRICK, J.A., HATTEN, J.A., PASTERNACK, G.B., GRAY, A.B., GONI, M.A., WHEATCROFT, R.A. (2012) The effects of wildfire on the sediment yield of a coastal California watershed. *GSA Bulletin* 124, 1130-1146.
- WELLS, W.G. II. (1987) The effects of fire on the generation of debris flows in southern California. *Reviews in Engineering Geology* 7, 105-113.
- Wing, S.L., Harrington, G.J., Smith, F.A., Bloch, J.I., Boyer, D.M., Freeman, K.H. (2005) Transient floral change and rapid global warming at the Paleocene-Eocene boundary. *Science* 310, 993-996.
- WRIGHT, J.D., SCHALLER, M.F. (2013) Evidence for a rapid release of carbon at the Paleocene-Eocene thermal maximum. *Proceedings of the National Academy of Sciences of the USA* 110, 15908-15913.
- ZEEBE, R.E., RIDGWELL, A., ZACHOS, J.C. (2016) Anthropogenic carbon release rate unprecedented during the past 66 million years. *Nature Geoscience* 9, 325-329.





 $$\odot 2019$$ The Authors Published by the European Association of Geochemistry

■ Widespread and intense wildfires at the Paleocene-Eocene boundary

M.K. Fung, M.F. Schaller, C.M. Hoff, M.E. Katz, J.D. Wright

Supplementary Information

The Supplementary Information includes:

- > Materials and Methods
- Supplementary Text
- Tables S-1 and S-2
- Figures S-1 to S-5
- Supplementary Information References

Materials and Methods

Samples of ~30-40 g dry weight (where available) were taken below and through the onset of the Paleocene-Eocene boundary carbon isotope excursion at Wilson Lake B (WL; 39.6598 °N, 75.0472 °W) and Randall's Farm (RF; 38.833 °N, 76.799 °W) cores. Sediment samples were soaked in DI water, washed through both 45 and 63 μ m sieves, and oven dried at 50 °C overnight. All sediment fines (<45 μ m) were saved from both sites.

We use scanning electron microscopy (SEM), Raman spectroscopy, and wavelength-dispersive X-ray spectroscopy (WDS) to identify the nature of the black grains and confirm that they are fossilised charcoal. Secondary electron images of representative charcoal pieces are made on a Zeiss EVO-MA15 scanning electron microscope at Union College in Schenectady, New York. For secondary electron imaging, all charcoal samples are sputter coated in gold-palladium. SEM imaging shows finely preserved plant anatomical features, characteristic of charcoal (Fig. S-2). Unlike charcoal, coal exhibits conchoidal fracture in SEM images (Glasspool and Scott, 2013). Raman spectra are collected using a Bruker SENTERRA Raman microscope with a 532 nm laser at Rensselaer Polytechnic Institute (RPI), are background-corrected, and compared to charcoal and graphite standards, and other maceral groups from Ulyanova et al. (2014) (Fig. S-4). WL and RF spectra are nearly identical to the charcoal standard and clearly distinct from the graphite standard. Furthermore, Ulyanova et al. (2014) observes a higher wavelength G-band and lower wavelength and narrower D1-band in the more ordered anthracite and coal spectra at 1580-1600 cm⁻¹ and 1350-1400 cm⁻¹ wavenumbers, respectively (Wang et al., 2014) compared to that of our charcoal. Our Raman results for the WL and RF material best match the charcoal standard. Resolution for Raman measurements is 1-3 cm⁻¹. WDS measurements are made using a Cameca SX-100 electron microprobe at RPI. Measurements of the black grains are done at 15 keV with a beam current of 20 nA with a Ni-C pseudocrystal to measure carbon. Samples were coated in platinum. The average standard deviation for individual carbon measurements is ~1 %. WDS measurements indicate the grains are 58-84 % carbon by weight (average ~74 %). The carbon content of bituminous coal and anthracite ranges from 86-98 %, Ulyanova et al. (2014), further supporting the charcoal nature of our material.

To calculate the abundance of charcoal throughout WL and RF, charcoal pieces were isolated through a sink-swim analysis technique where charcoal pieces were floated in a solution of lithium metatungstate (LMT) gravimetrically diluted to a density of



2.2 g/cm³. Individual charcoal grains were counted in the >63 μ m size fraction for charcoal abundance and normalised per gram dry sediment. These counts were checked by manual picking of an entire unfloated sample. Samples from this size fraction allow us to observe anatomical plant structure, further ensuring the material is charcoal. We find that our sink-swim technique recovers about 81 % of the charcoal that could be visually identified and separated by manually picking a sample. The δ^{13} C_{charcoal} is measured at RPI on an Elementar ISOTOPE Select elemental analyser (EA) coupled to an Isoprime 100 isotope ratio mass spectrometer (IRMS) run in continuous flow mode. The NBS22 standard was analysed multiple times in each sample run, with a 2σ analytical error of 0.12 % in the weight range of the charcoal grains. The δ^{13} C_{charcoal} presented here are made on a random selection of 4-12 μ g of ~20 charcoal grains isolated from a single sample. Manually and physically separating the charcoal from the bulk sample ensures that we analyse a consistent carbon-bearing phase through the section.

By individually picking or physically separating charcoal pieces for isotope analysis, as opposed to the bulk processing techniques used in previous studies (Moore and Kurtz, 2008), we ensure that the material we analyse remains consistent throughout the section and also between sites. Furthermore, we confirm that the isotope values we report have been measured on fossil charcoal and not another organic phase.

Reflectance measurements were contracted to Maria Mastalerz at Indiana University, and were made on individual charcoal fragments to infer the temperature of formation. Due to feasibility issues (cost, size, difficulty in polishing), measurements were completed on only 7 fragments from both sites. Petrographic observations and reflectance analyses were carried out in a Leica DM 2500P reflected-light microscope linked to a TIDAS PMT IV photometric system. Maceral groups were identified based on their optical characteristics (morphology, cell structure preservation, reflectance, etc.) For maceral reflectance analysis (R_0 random), 25 measurements were averaged.

Supplementary Text

Characterising the P-E Charcoal

Charcoal deposition in marine sediments is controlled primarily by fire frequency and secondarily by wind transport of charcoal from land to ocean (Herring, 1985), with more wildfire activity resulting in higher charcoal flux to marine sediments. At both WL and RF, the anomalous abundance of fossilised charcoal that occurs above the P-E spherule layer indicates that increased wildfire activity followed the extraterrestrial impact. Direct comparison of our charcoal abundance data to other shallow-marine deposits is challenging, because of the scarcity of methodological studies on lower Tertiary charcoalified plant deposits (Scott, 2000). For example, studies examining charcoal fluxes into marine sediments during the Cenozoic measured charcoal concentrations through bulk extraction techniques on the entire sediment sample (Herring, 1985), in contrast to our charcoal abundance counts which are constrained to the 63-150 µm size fraction. Furthermore, documented charcoal flux rates as old as the P-E boundary are rare (Herring, 1985). This problem is further exacerbated by the lack of systematic standardisation of both identification and analytical quantification of charcoal in different environments (Schmidt and Noack, 2000).

The use of chemical methods to quantify black carbon is most frequently employed, but is not an exact measure of charcoal (Scott, 2010). Graphitic black carbon (GBC) at the farther offshore Bass River Site (ODP 174AX) shows a $\delta^{13}C_{GBC}$ excursion that appears to be coincident with the CIE onset in bulk calcium carbonate (Moore and Kurtz, 2008); however, these results are not comparable to our $\delta^{13}C_{charcoal}$ for several reasons. Moore and Kurtz (2008) use a bulk extraction method to isolate GBC, which can incorporate GBC of different origins along with unrelated organics, leading to a mixed signal from multiple sources. Furthermore, wildfires are not the sole source of GBC (Goldberg, 1985), whereas charcoal on the shelf is exclusively of wildfire origin (Belcher *et al.*, 2003). Our δ^{13} C measurements were performed only on individual fragments confirmed to be charcoal (see Fig. S-2), thereby eliminating contamination from bulk sedimentary constituents. If the GBC is indeed evidence of wildfires, its coincidence with the CIE onset in bulk carbonate is consistent with a much lower sedimentation rate at the Bass River (BR) site (Stassen *et al.*, 2012). We note that the offset between the CIE in charcoal and the CIE in carbonate is variable and increases with decreasing water depth at WL and RF, where BR may be the offshore end-member.

We note that when plotted by depth, events 1 and 2 on Figure 3 appear further apart at RF than at WL; this is likely an artifact of the much lower sampling resolution and higher sedimentation rate at RF compared to WL and the ~61 cm sampling gap between the sample containing the apparent charcoal peak and the sample immediately below. The larger separation between peaks at RF compared to WL is also consistent with a higher sedimentation rate at the shallower, more proximal (close to shoreline) site (similar to relationships in modern coastal regions (Kuehl *et al.*, 1986)).

We compare our charcoal results to magnetic records using the ratio of saturation remanence to saturation magnetization (M_r/M_s) at WL (Kent *et al.*, 2017) and ferromagnetic resonance spectroscopy (FMR α) at RF (Kopp *et al.*, 2009). These two magnetic parameters are related indicators of single domain magnetite, and M_r/M_s measured elsewhere in the Marlboro Clay at Ancora and



Bass River (Kent *et al.*, 2003) show coincident changes with FMR α (Kopp *et al.*, 2007; 2009). The increase in magnetic nanoparticles near the base of the Marlboro Clay extends even farther than the charcoal record at WL and RF, as documented in sites across the Salisbury Embayment from northern New Jersey to southern Virginia (~400 km) (Kopp *et al.*, 2009; Kent *et al.*, 2003; Lanci *et al.*, 2002), indicating that the wildfires were regionally widespread and synchronous (within the level of resolution possible).

Vegetation that remains dead for a long period of time before burning can exhibit pre-charring biodegradation (Jones and Lim, 2000). None of the charcoal fragments that we imaged display features characteristic of biodegradation, such as perforations and trackways, indicating that there was no significant delay between P-E plant death and conversion to charcoal. This lack of delay does not discount the possibility that the P-E charcoal formed when the remains of plants perished from "ordinary" causes (*i.e.* not the victim of an extraterrestrial impact) and simply died from hotter, dryer climate conditions, and eventually turned into charcoal as the result of intense widespread wildfires ignited by a common method (*e.g.*, lightning).

Linking Wildfires and Extraterrestrial Impacts

Following the Cretaceous-Paleogene boundary (K-Pg) impact event, a global K-Pg soot layer was produced by combustion of large amounts of vegetation in a firestorm ignited by an extraterrestrial impact (Wolbach *et al.*, 1985; 1990a; 1990b; Venkatesan and Dahl, 1989). Thermal radiation and ejecta fallout from the K-Pg impact likely ignited widespread wildfires (Shuvalov, 2001). Impact models demonstrate that the necessary thermal radiation could have originated from: 1) hot, compressed air released by the shockwave; 2) the vapor plume (composed of vaporised impactor and target rock, called the "fireball"); and 3) re-entry and fallout of ejecta sufficient to ignite massive wildfires (Melosh *et al.*, 1990; Collins et al., 2005; Kring and Durda, 2002; Durda and Kring 2004). The occurrence of wildfires is also supported by a "fern spike" (Tschudy *et al.*, 1984), as well as a dramatic increase in fusain (fossil charcoal) following the K-Pg boundary near the impact site (Kruge *et al.*, 1994), although the global nature of fusain deposition has not been established. The lack of above-background charcoal levels in the U.S. Western Interior and abundance of non-charred plant fragments in K-Pg material suggests the wildfires may have been widespread but only regional, although this apparent deficiency of charcoal may have been interpreted due to incorrect sedimentation rates (see Roberston *et al.*, 2013 cf. Belcher *et al.*, 2003 and Scott *et al.*, 2000). Furthermore, Jones and Lim (2000) found evidence of biodegradation in 53 % of charcoal fragments examined from K-Pg sites, suggesting time lag between plant mortality and subsequent burning. Nonetheless, a comparison of our results to the sequence of K-Pg events is beneficial, as we unequivocally show above-background levels of charred plant material (charcoal) at the P-E boundary.

Marlboro Clay

Recently formed charcoal has a density less than water and initially floats (Nichols *et al.*, 2000). The buoyancy of the charcoal grains (which keeps the particles suspended until becoming waterlogged (Vaugh and Nichols, 1995; Rhodes, 1996), compared to the greater density of the clay particles explains why the charcoal peak is slightly above the base of the clay. Major storm events produce fluidised mudflows composed of suspended sediment that are eventually deposited in the inner shelf (Geyer *et al.*, 2000; Goff *et al.*, 2013). Additionally, in modern California, rapidly developed hyperpycnal sediment gravity currents deposit massive amounts of fluidised mud, formed within hours following moderately sized river discharge events (Warrick *et al.*, 2007). Mudflow densities are >2.0 g/cm³ due to increased sediment load (Woolley, 1946; Sharp and Nobles, 1963). Considerable density stratification occurs due to the excess density of these mudflows (Ross and Mehta, 1989). Therefore, it is possible that the less dense charcoal floated within the mudflows, creating the observed offset in the charcoal abundance and clay boundary level.

We consider Marlboro Clay sedimentation rates and duration for the CIE onset using end-member scenarios (Table S-2) to provide context for our findings. An independent submillennial-scale CIE onset for Site 690 using a cyclostratigraphic age model is also shown for perspective (Röhl *et al.*, 2007). Because there is no agreement on the sedimentation rate of the Marlboro Clay at the CIE onset, it is difficult to provide a timeline for our order of events. Even though our findings cannot provide precise timing for the CIE onset, an important result is that they do not support a millennial onset. Such a timeframe would require no plant growth for thousands of years and a widespread spike in wildfire activity that is temporally unrelated to the onset of the CIE, making its origin ambiguous.



Supplementary Tables

Table S-1 Reflectance measurements (R_o) and corresponding temperature of formation (Scott and Jones, 1991) for samples from WL and RF. Highest R_o values, and inferred formation temperatures come from the charcoal peaks at both RF and WL sites.

Site	Depth (ft)	Depth (m)	Average Reflectance R ₀	Temperature (°C)*
RF	63.5	19.35	1.24	341
RF	65.5	19.96	0.64	267
RF	74.9	22.83	0.76	283
WL	354.9	108.17	0.86	295
WL	365.1	111.28	1.10	324
WL	365.8	111.50	2.99	552
WL	366.6	111.74	0.38	237

Table S-2 Comparison of sedimentation rates and duration of the CIE onset from multiple palaeo-shelf sites and a deep-sea site. Paleodepth ranges for sites are shown.

	Salisbury	Deep Sea		
Study:	Wright and Schaller (2013)	Self-Trail et al. (2017)	Zeebe et al. (2016)	Rohl <i>et al.</i> (2007)
Site:	Millville and Wilson Lake B (~59 and ~39 m)	Mattawoman Creek- Billingsley Road (MCBR) (~10-30 m)	Millville (~59 m)	Site 690 (1800 m)
Sedimentation Rate:	2 cm yr ⁻¹	50 cm kyr ⁻¹	6.2 cm kyr ⁻¹	1.3 cm kyr-1
CIE Duration:	~13 yr	4 kyr	4 kyr	<750 yr



Supplementary Figures

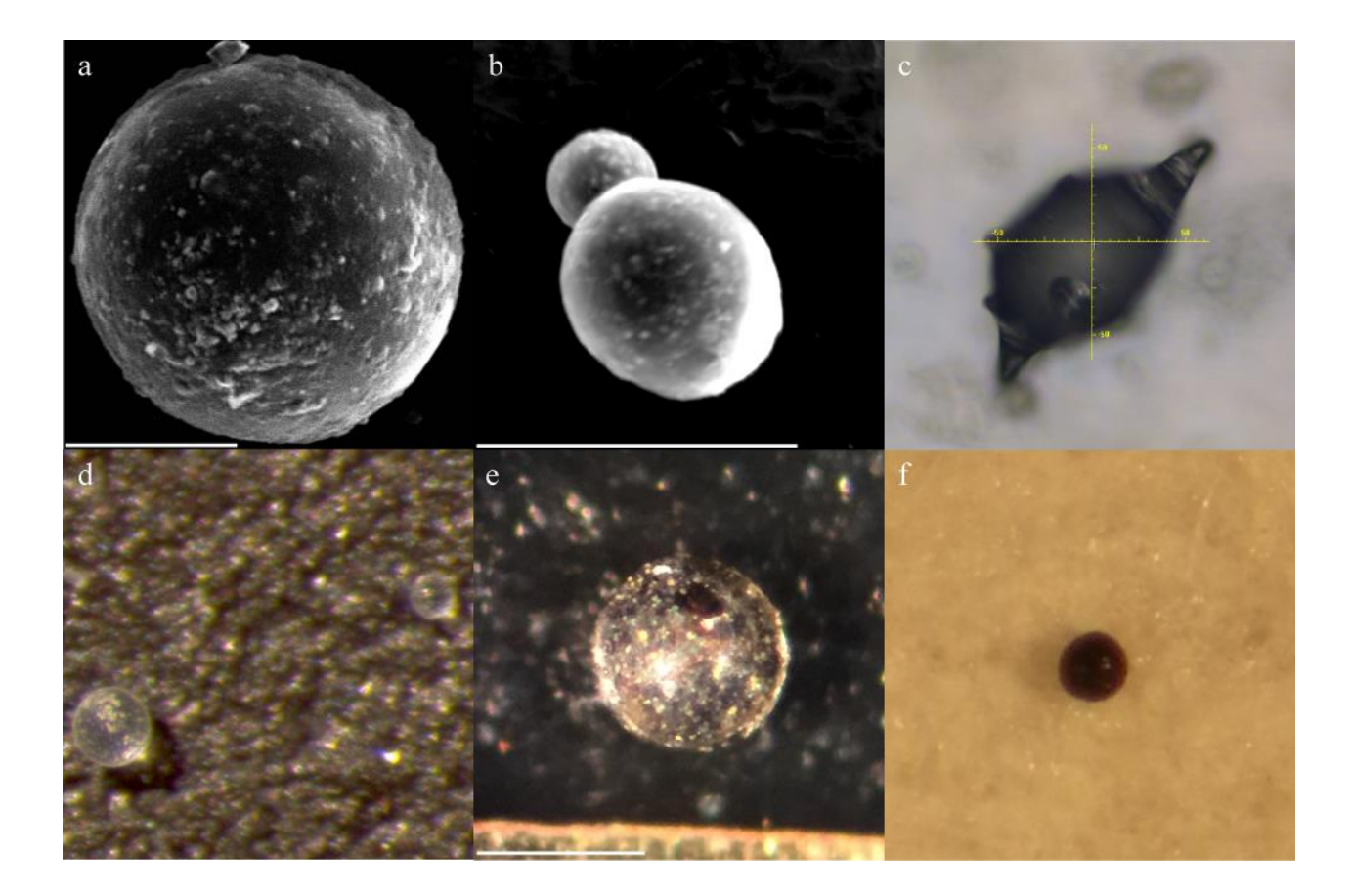


Figure S-1 SEM (a-b) and light micrograph (c-f) images of RF spherules. White scale bar is 50 microns. See Schaller *et al.* (2016) and Schaller and Fung (2018) for detailed physical and chemical descriptions of spherules at other sites. Note, spherules from RF were some of the very first identified and much of the material was expended during the initial characterisation stage. These spherules were imaged prior to using a white picking tray.



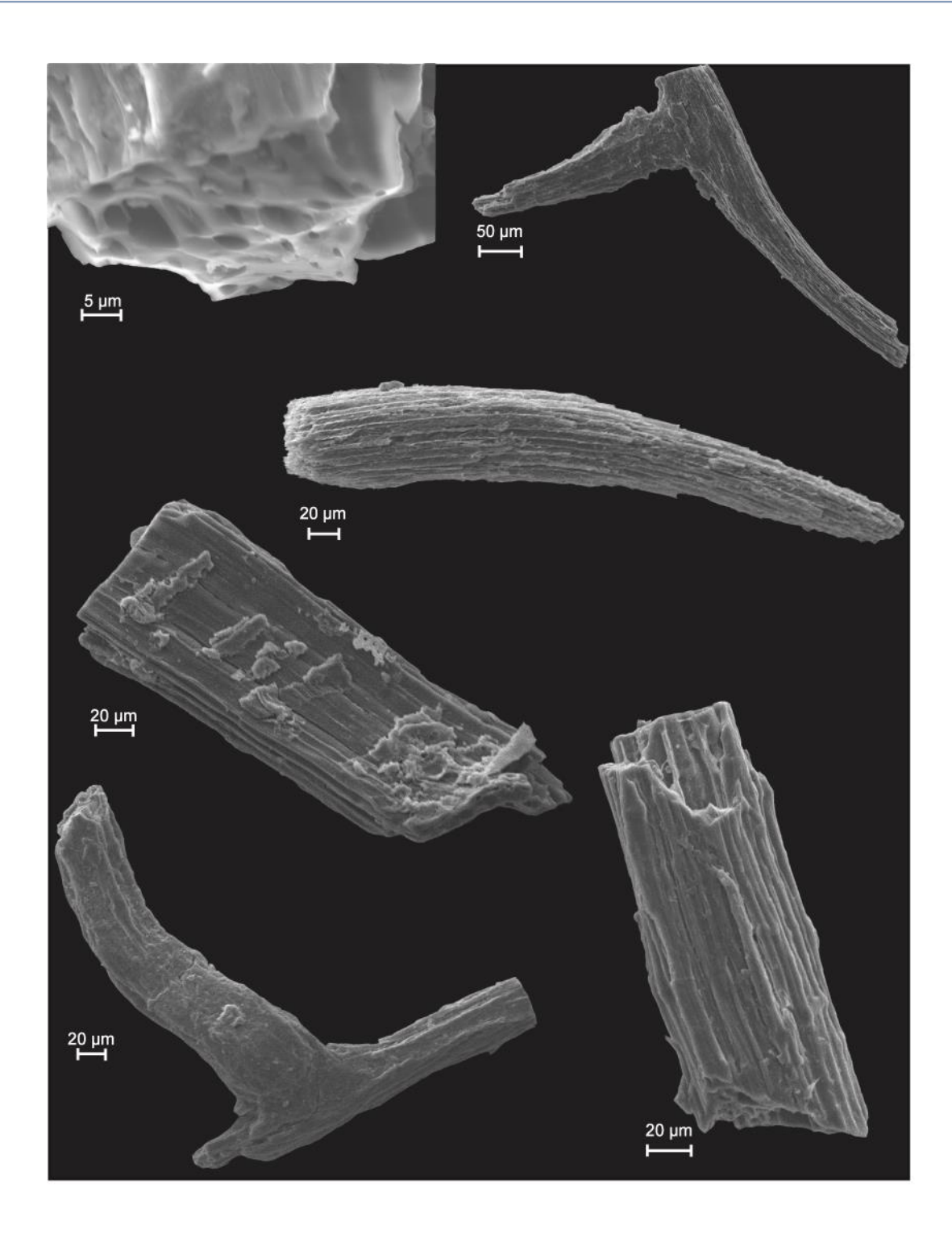


Figure S-2 SEM images of representative charcoal fragments from WL and RF reveal elongate xylem fibers, detailed tracheid cells, smooth homogenised cell walls, and well-preserved internal honeycomb structures. Working distances range from 5-24 mm and EHT is set at 15 kV.



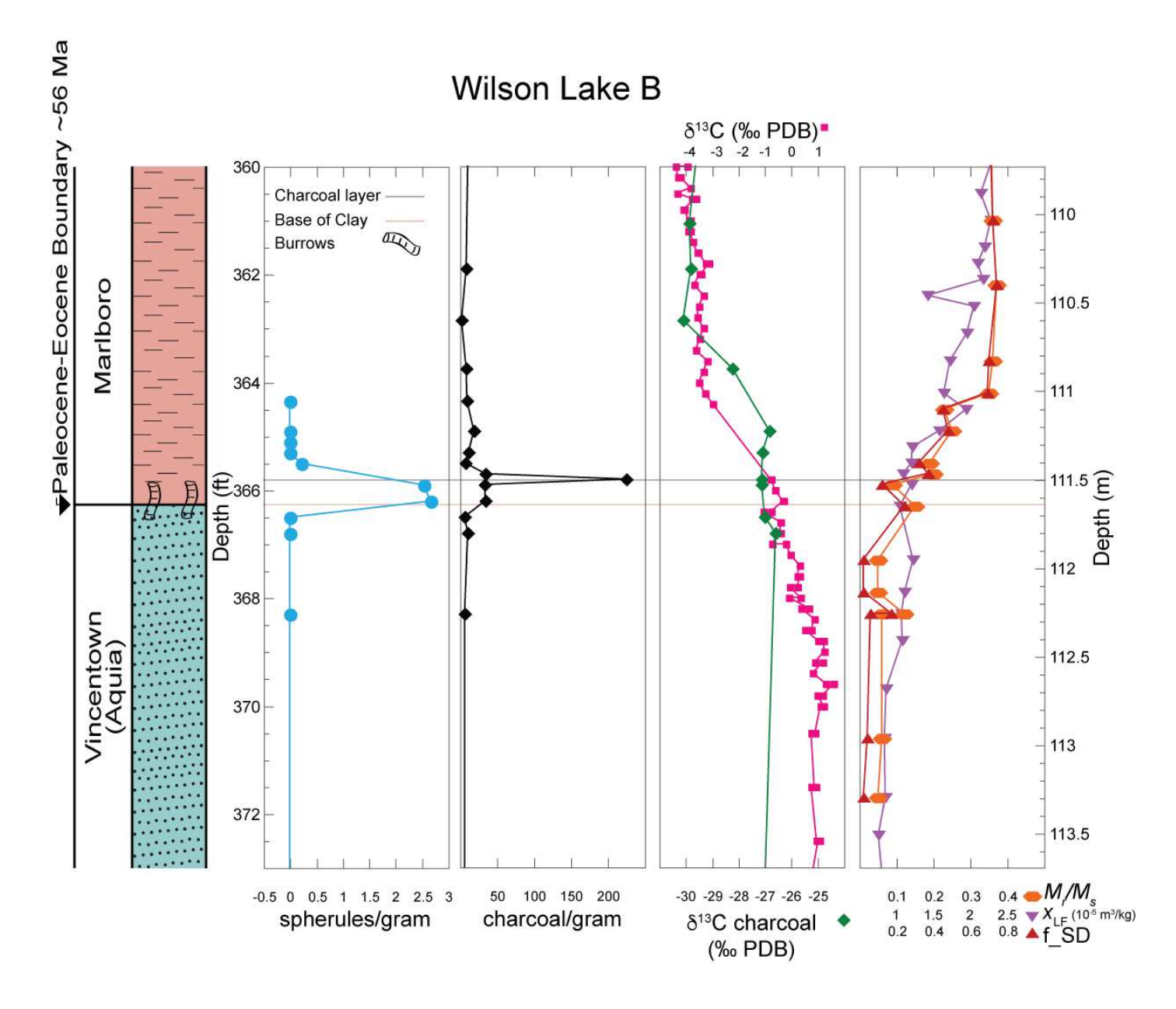


Figure S-3 Expanded CIE onset at WL. Charcoal abundance and $\delta^{13}C_{charcoal}$ plotted with $\delta^{13}C_{bulk}$ and spherules/gram discovered at WL. Ratio of saturation remanence to saturation magnetization (M_r/M_s), low-field magnetic susceptibility (X_{LF}), and volume weighted SD fraction (f_SD) at WL (Kent *et al.*, 2017) illustrates how the abrupt rise in magnetization is coincident with the increase in charcoal abundance.



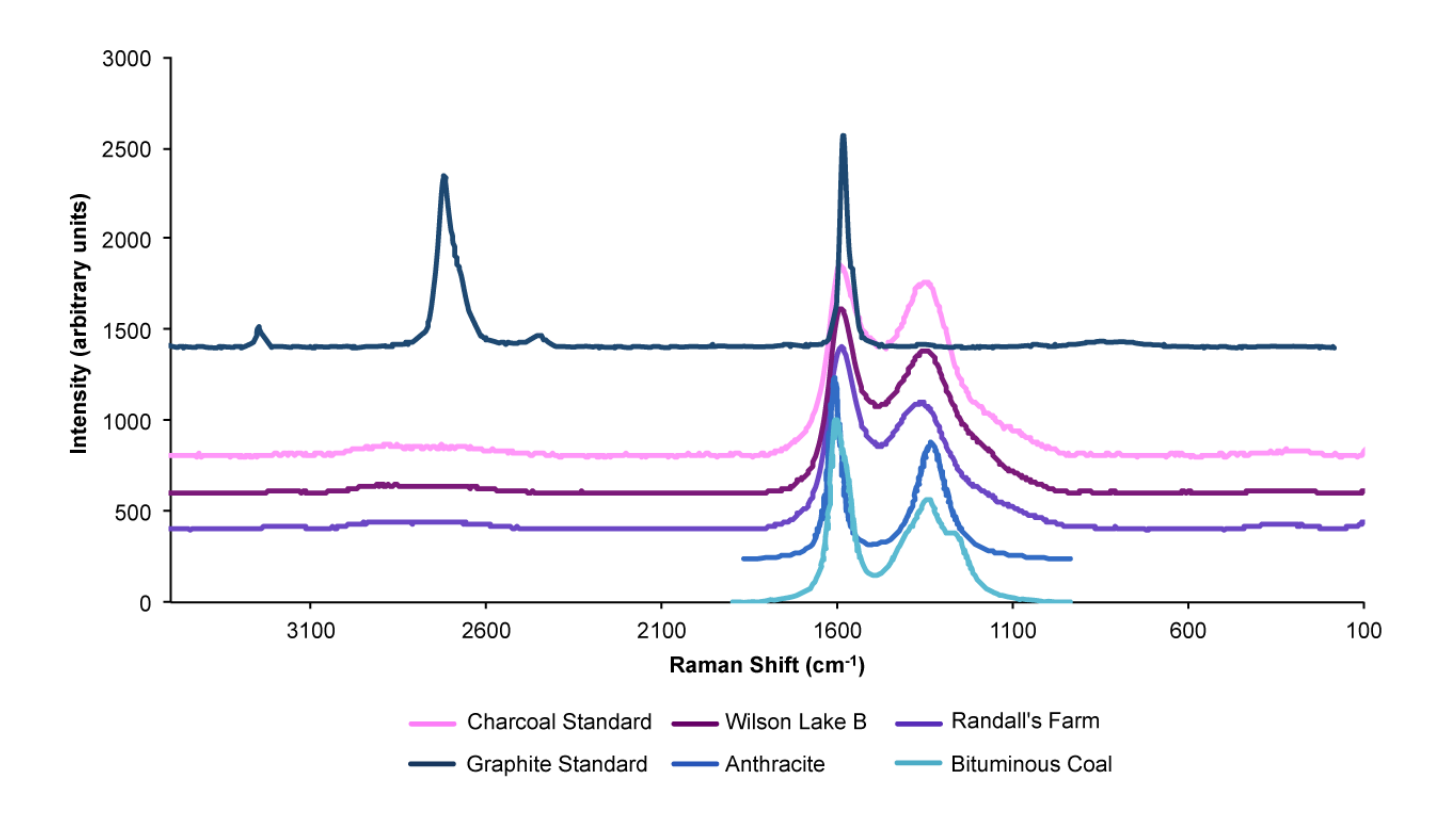


Figure S-4 Raman spectra of representative charcoal pieces from WL and RF, compared to a wood charcoal standard, graphite (RRUFF IDR050503), anthracite (Ulyanova et al., 2014), and bituminous coal (Ulyanova et al., 2014). Raman spectra from Ulyanova et al. (2014) are presented in the 900-1900 cm⁻¹ wavenumber range.

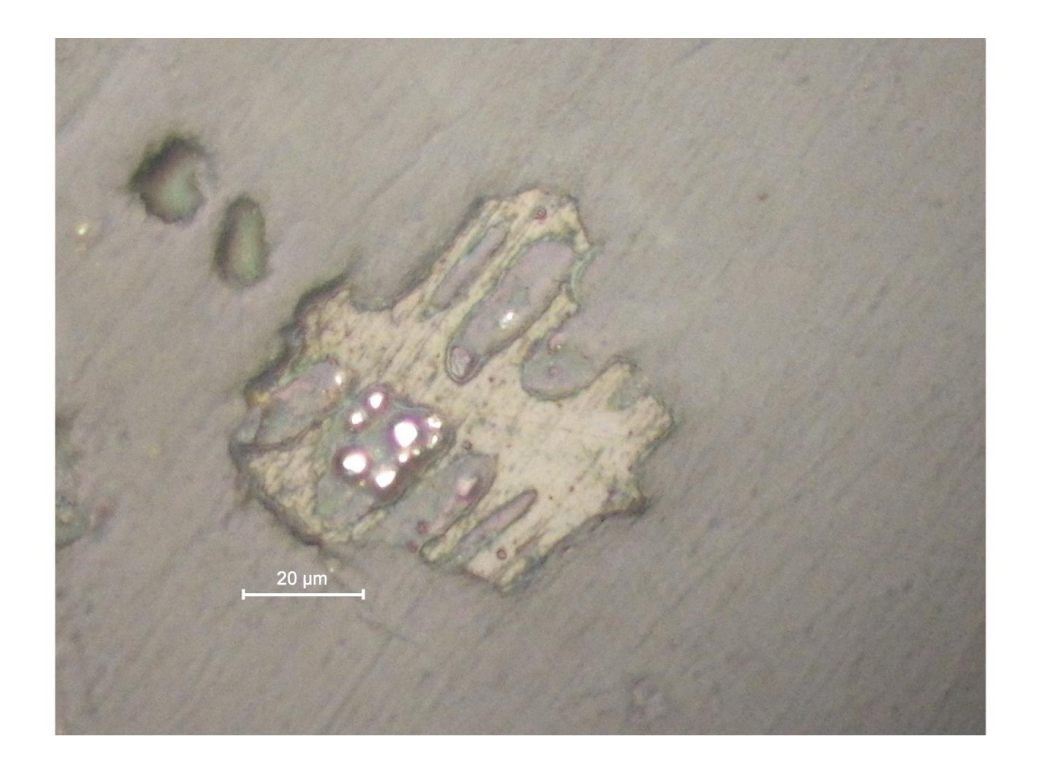


Figure S-5 Representative images of polished charcoal fragments from WL and RF. Note smooth, well-preserved cell walls present in the samples. Bright areas are post-depositional pyrite.



Supplementary Information References

- Belcher, C.M., Collinson, M.E., Sweet, A.R., Hildebrand, A.R., Scott, A.C. (2003) Fireball passes and nothing burns The role of thermal radiation in the Cretaceous-Tertiary event: Evidence from the charcoal record of North America. *Geology* 31, 1061-1064.
- Collins, G.S., Melosh, H.J., Marcus, R.A. (2005) Earth Impact Effects Program: A Web-based computer program for calculating the regional environmental consequences of a meteoroid impact on Earth. *Meteoritics & Planetary Science* 40, 817-840.
- Durda, D.D., Kring, D.A. (2004) Ignition threshold for impact-generated fires. Journal of Geophysical Research 109, 1-14.
- Geyer, W.R., Hill, P., Milligan, T., Traykovski, P. (2000) The structure of the Eel River plume during foods. Continental Shelf Research 20, 2067-2093.
- Glasspool, I.J., Scott, A.C. (2013) Identifying Past Fire Events. In: Belcher, C. M. (Eds.) Fire Phenomena and the Earth System: An Interdisciplinary Guide to the Fire Science. John Wiley & Sons, Ltd, Chichester, 179-206.
- Goff, J.A. et al. (2013) Rapid Response Survey Gauges Sandy's Impact on Seafloor. EOS 94(39), 337-348.
- Goldberg, E.D. (1985) Black Carbon in the Environment: Properties and Distribution. John Wiley, New York.
- Herring. J.R. (1985) Charcoal fluxes into sediments of the North Pacific Ocean: the Cenozoic record of burning. In: Sundquist, E.T., Broecker, W.S. (Eds) The Carbon Cycle and Atmospheric CO2: Natural Variations Archean to Present. *Geophysical Monograph*. 419-442.
- Jones, T.P., Lim, B. (2000) Extraterrestrial impacts and wildfires. Palaeogeography, Palaeoclimatology, Palaeoecology 164, 57-66.
- Kent, D.V., Cramer, B.S., Lanci, L., Wang, D., Wright, J.D., Van der Voo, R. (2003) A case for a comet impact trigger for the Paleocene/Eocene thermal maximum and carbon isotope excursion. Earth and Planetary Science Letters 211, 13-26.
- Kent, D.V., Lanci, L., Wang, H., Wright, J.D. (2017) Enhanced magnetization of the Marlboro Clay as a product of soil pyrogenesis at the Paleocene-Eocene Boundary? Earth and Planetary Science Letters 473, 303-312.
- Kring, D.A., Durda, D.D. (2002) Trajectories and distribution of material ejected from the Chicxulub impact crater: Implications for postimpact wildfires. *Journal of Geophysical Research* 107, 6-22.
- Kruge, M.A., Stankiewicz, A.B., Crelling, J.C., Montanari, A., Bensley, D.F. (1994) Fossil Charcoal in Cretaceous-Tertiary boundary strata: Evidence for catastrophic firestorm and megawave. *Geochimica et Cosmochimica Acta* 58, 1393-1397.
- Kuehl, S.A., DeMaster, D.J., Nittrouer, C.A. (1986) Nature of sediment accumulation on the Amazon continental shelf. Continental Shelf Research 6, 209-225.
- Lanci, L., Kent, D.V., Miller, K.G. (2002) Detection of Late Cretaceous and Cenozoic sequence boundaries on the Atlantic coastal plain using core log integration of magnetic susceptibility and natural gamma ray measurements at Ancora, New Jersey. *Journal of Geophysical Research* 107, 2216.
- Melosh, H.S., Schneider, N.M., Zahnlek, J., Latham, D. (1990) Ignition of global wildfires at the Cretaceous/Tertiary boundary. Nature 343, 251-254.
- Moore, E.A., Kurtz, A.C. (2008) Black carbon in Paleocene-Eocene boundary sediments: A test of biomass combustion as the PETM trigger. *Palaeogeography, Palaeoclimatology, Palaeocology* 267, 147-152.
- Nichols G.J., Cripps J.A., Collinson M.E., Scott A.C. (2000) Experiments in waterlogging and sedimentology of charcoal: results and implications. *Palaeogeography, Palaeclimatology, Palaeecology* 164, 43-56.
- Rhodes, A.N. (1996) Moorland Fire History from Microscopic Charcoal in Soils and Lake Sediments. PhD Thesis. University of Newcastle upon Tyne, 25-26.
- Robertson, D.S., Lewis, W.M., Sheehan, P.M., Toon, O.B. (2013) K-Pg extinction: Reevaluation of the heat-fire hypothesis. *Journal of Geophysical Research: Biogeosciences* 118, 329-336.
- Röhl, U., Westerhold, T., Bralower, T.J., Zachos, J.C. (2007) On the duration of the Paleocene–Eocene thermal maximum (PETM). Geochemistry Geophysics Geosystems 8, 1-
- Ross M.A., Mehta, A.J. (1989) On the Mechanics of Lutoclines and Fluid Mud. Journal of Coastal Research 5, 551-62.
- Self-Trail, J. M., et al. (2017) Shallow marine response to global climate change during the Paleocene-Eocene Thermal Maximum, Salisbury Embayment, USA. Paleoceanography 32, 710-728.
- Schaller, M.F., Fung, M.K., Wright, J.D., Katz, M.E., Kent, D.V. (2016) Evidence of an Extraterrestrial Impact at the Paleocene-Eocene boundary. Science 354, 225-229.
- Schaller, M.F., Fung, M.K. (2018) The extraterrestrial impact evidence at the Paleocene-Eocene boundary and sequence of environmental change on the continental shelf. Philosophical Transactions of the Royal Society A 376, doi: 10.1098/rsta.2017.0081.
- Schmidt, M.W., Noack, A.G. (2000) Black carbon in soils and sediments: Analysis, distribution, implications, and current challenges. *Global Biogeochemical Cycles* 14, 777-793
- Scott, A.C. (2000) The Pre-Quaternary history of fire. Palaeogeography, Palaeoclimatology, Palaeoecology 164, 281-329.
- Scott, A.C. (2010) Charcoal recognition, taphonomy and uses in palaeoenvironmental analysis. Palaeogeography, Palaeoclimatology, Palaeoecology 291, 11-39.
- Scott, A.C., Jones, T.P. (1991) Microscopic observations of Recent and fossil charcoal. Microscopy and Analysis 25, 13-15.
- Scott, A.C., Lomax, B.H., Collinson, M.E., Upchurch, G.R., Beerling, D.J. (2000) Fire across the K-T boundary: initial results from the Sugarite Coal, New Mexico, USA. Palaeogeography, Palaeoclimatology, Palaeoecology 164, 381-395.
- Sharp, R.P., Nobles, L.H. (1963) Mudflow of 1941 at Wrightwood, Southern California. Bulletin of the Geological Society of America 64, 547-560.
- Shuvalov, V.V. (2001) Radiation effects of the Chicxulub impact event. In: Buffetaut, E., Koeberl, C (Eds) Geological and biological effects of impact events. Springer, Berlin, Federal Republic of Germany, 237-247.
- Stassen, P., Thomas, E., Speijer, R.P. (2012) The progression of environmental changes during the onset of the Paleocene-Eocene thermal maximum (New Jersey Coastal Plain). *Austrian Journal of Earth Sciences* 105, 169-178.
- Tschudy, R.H., Pillmore, C.L., Orth, C.J., Gilmore, J.S., Knight, J.D. (1984) Disruption of the terrestrial plant ecosystem at the Cretaceous-Tertiary boundary, Western Interior. Science 225, 1030-1032.
- Ulyanova, E.V., Molchanov, A.N., Prokhorov, I.Y., Grinyov, V.G. (2014) Fine structure of Raman spectra in coals of different rank. *International Journal of Coal Geology* 121, 37-43.
- Vaughn, A., Nichols, G. (1995) Controls on the deposition of charcoal: implications for sedimentary accumulations of fusain. *Journal of Sedimentary Research* A65(1), 129-135
- Venkatesan, M.I., Dahl, J. (1989) Organic geochemical evidence for global fires at the Cretaceous/Tertiary boundary. Nature 338, 57-60.
- Wang, S., Cheng, H., Jiang, D., Huang, F., Su, S., Bai, H. (2014) Raman spectroscopy of coal component of Late Permian coals from Southern China. Spectroscopy 132, 767-770.



Warrick, J.A., Xu, J., Noble, M.A., Lee, H.J. (2007) Rapid formation for hyperpycnal sediment gravity currents offshore of a semi-arid California river. Continental Shelf Research 28, 991-1009.

Wolbach, W.S., Lewis, R.S., Anders, E. (1985) Cretaceous extinctions; Evidence for wildfires and search for meteoritic material. Science 230, 167-170.

Wolbach, W.S., Anders, E., Nazarov., M.A. (1990a) Fires at the K/T boundary: Carbon at the Sumbar, Turkmenia, site. Geochimica et Cosmochimica Acta 54, 1133-1146.

Wolbach, W.S., Gilmour, I., Anders, E. (1990b) Major wildfires at the K-T boundary. In: Sharpton, V.L., Ward, P.D. (Eds.) Global Catastrophes in Earth History. GSA Special Paper, Boulder, CO, 247, 391-400.

Woolley, R.R. (1946) Cloudburst floods in Utah 1850-1938. U.S. Geological Survey, W.S. Paper 994, 1-128.

Wright, J.D., Schaller, M.F. (2013) Evidence for a rapid release of carbon at the Paleocene-Eocene thermal maximum. PNAS 110, 15908-15913.

Zeebe, R.E., Ridgwell, A., Zachos, J.C. (2016) Anthropogenic carbon release rate unprecedented during the past 66 million years. Nature Geoscience 9, 325-329.

